ORIGINAL PAPER

Ultra-depleted, shallow cratonic mantle beneath West Greenland: dunitic xenoliths from Ubekendt Ejland

Stefan Bernstein · Karen Hanghøj ·
Peter B. Kelemen · C. Kent Brooks

Abstract Dunitic xenoliths from late Palaeogene, alkaline basalt flows on Ubekendt Ejland, West Greenland contain olivine with $100 \times Mg/(Mg + Fe)$, or Mg#, between 92.0 and 93.7. Orthopyroxene has very low Al_2O_3 and CaO contents (0.024–1.639 and 0.062–0.275 wt%, respectively). Spinel has $100 \times Cr/(Cr + Al)$, or Cr#, between 46.98 and 95.67. Clinopyroxene is absent. The osmium isotopic composition of olivine and spinel mineral separates shows a considerable span of $^{187}Os/^{188}Os$ values. The most unradiogenic $^{187}Os/^{188}Os$ value of 0.1046 corresponds to a Re-depletion age of ca. 3.3 Gy, while the most radiogenic value of 0.1336 is higher than present-day chondrite. The Os isotopic composition of the xenoliths is consistent with their origin as restites from a melt extraction event in the Archaean, followed by one or more subsequent metasomatic event(s). The high Cr# in spinel and low modal pyroxene of the Ubekendt Ejland xenoliths are similar to values of some highly depleted mantle peridotites from arc settings. However, highly depleted, arc-related peridotites have higher Cr# in spinel for a given proportion of modal olivine, compared to cratonic xenolith suites from Greenland, which instead form coherent trends with abyssal peridotites, dredged from modern mid-ocean ridges. This suggests that depleted cratonic harzburgites and dunites from shallow lithospheric mantle represent the residue from dry melting in the Archaean.

Communicated by I. Parsons

S. Bernstein (✉)
Geological Survey of Denmark and Greenland,
ØsterVoldgade 10, 1350 Copenhagen K, Denmark
e-mail: sb@geus.dk

S. Bernstein
Arctic Station, 3953 Qeqertarsuaq, Greenland

K. Hanghøj · P. B. Kelemen
Lamont-Doherty Earth Observatory, Columbia University,
PO Box 1000, Palisades, NY 10964-8000, USA

C. K. Brooks
Geological Institute, University of Copenhagen,
Øster Voldgade 10, 1350 Copenhagen K, Denmark

Introduction

Studies of mantle xenolith suites from Archaean cratons have shown that cratonic lithospheric mantle is generally strongly depleted in basaltic components and has high Mg# (= $100 \times Mg/(Mg+Fe)$), and is thus inferred to represent the residue after ancient melt extraction events (e.g. Boyd and Mertzman 1987; Boyd 1989; Menzies 1990; Pearson 1999; Herzberg 2004). The type examples of xenolith suites from cratonic mantle have long been taken as those of the Kaapvaal craton in South Africa, but the orthopyroxene-rich nature of xenoliths from the Kaapvaal cratonic mantle has been problematic to understand, in the context of mantle melting (Boyd 1989; Walter 1998; Kelemen et al. 1998; Herzberg 2004). It has recently been demonstrated that some portions of the cratonic mantle are orthopyroxene-poor, while maintaining their high Mg#. Orthopyroxene-poor harzburgite xenoliths from Wiedemann Fjord in East Greenland, with Archaean Re-depletion ages (Hanghøj et al. 2000), are probably residues after about 40% melting of a fertile mantle composition (Bernstein et al. 1998). Similar,

orthopyroxene-poor, high Mg# residues are found in the West Greenland kimberlite fields (Bizzarro and Stevenson 2003) as well as in other cratons such as the Canadian Northwest Territories (Boyd and Canil 1997; Kopylova et al. 1999) and Tanzania (Lee and Rudnick 1999). Here we report on another orthopyroxene-poor mantle xenolith suite, from Ubekendt Ejland in West Greenland (Larsen 1982). The presence of the Ubekendt Ejland xenoliths, together with similar samples from the other West Greenland and Wiedemann Fjord localities, suggests that orthopyroxene-poor, high Mg# peridotite may be the dominant lithology in the shallow portion of the Greenland cratonic mantle.

In this paper, we discuss the origin of these orthopyroxene-poor xenoliths. We also relate the modal composition and mineral chemistry of the xenolith suites from Ubekendt Ejland and Wiedemann Fjord to mantle peridotites with similar characteristics from recent or present-day arc settings. This provides constraints on the hydrous or anhydrous nature of the melt extraction event that depleted the shallow cratonic mantle beneath Greenland.

Occurrence of ultramafic nodules on Ubekendt Ejland

Ubekendt Ejland is dominated by early Palaeogene volcanics and intrusive rocks (Drever and Game 1948; Larsen 1977a, b) (Fig. 1). Most of the island is composed of picritic and olivine-phyric lavas, hyaloclastites and volcanic breccias, belonging to the Vaigat Formation. The Vaigat Formation is overlain by plagioclase-phyric basaltic lavas and tuffs, the lower basaltic sequence of which belongs to the Maligât Formation, while the pyroclastic units are probably younger (Larsen 1977b). The succession of lava formations on Ubekendt Ejland terminates with the Erqua Formation of Eocene age (Drever and Game 1948, Larsen 1977a, b), which consists of olivine- and clinopyroxene-phyric alkali basalts (Larsen 1977b). In one of the basaltic flows of the Erqua Formation, Clarke (1973) and Larsen (1982) reported the occurrence of ultramafic nodules. During fieldwork in 1997 and 1999, scarce ultramafic nodules were found in two more flows, one at the base and one at the top of the Erqua Formation, outcropping at Eqqua (new spelling, Fig. 1). The main occurrence of the nodules is, however, in the basalt flow reported by Clarke (1973) and Larsen (1982), from which more than 100 ultramafic nodules were recovered for this study.

As described by Bernstein and Brooks (1999), the ultramafic nodules form two groups. One consists mainly of wehrlites with cumulate textures. The other consists of dunites with metamorphic textures. The wehrlite nodules generally lack orthopyroxene (only present in one sample) and have olivines with Mg# between 79.90 and 91.25, while the dunite nodules lack clinopyroxene, more than half include small amounts of orthopyroxene, and all have olivine Mg# between 92.0 and 93.7% (Fig. 2). The lower Mg# in olivine and their cumulate textures suggests that the low-Mg# group of xenoliths are cumulates from primitive melts and thus, perhaps, of Palaeogene origin like the lavas of Ubekendt Ejland. This paper focuses on the group of high Mg#, dominantly dunitic xenoliths. On the basis of their compositions and textures, we interpret these xenoliths as representing samples of the lithospheric mantle (Bernstein and Brooks 1999). In the present collection, 31 samples belong to this group of xenoliths.

Analytical techniques

Minerals grains were analysed on standard polished thin sections, using the JEOL electron microprobe at the Geological Institute, University of Copenhagen. All elements were measured by WDS, with 20 s peak count time for Na, Mg, Fe, Si and Ti, while Cr, Ni, Ca and Al were measured with 40 s peak count time. Background count time on either side of the peak was half that of peak count time. Table 1 lists all mineral data, which represent the average of at least three analyses in each of three individual mineral grains. Mineral modes were determined by point counting.

Seven xenoliths were analysed for Os isotopic compositions using the Carius tube technique (Shirey and Walker 1995). Hand-picked separates of olivine or/ and spinel were carefully cleaned and digested in inverse aqua regia in sealed glass tubes (Carius tubes) for > 72 h at 200°C. Subsequently, samples were distilled twice to extract the osmium. Samples were loaded onto Ni filaments and analysed by N-TIMS at the University of Copenhagen. The Os blank for the Carius tube technique is 2.8 pg/g sample, and samples have not been blank corrected. Analyses are given in Table 2. Due to laboratory problems during the separation of Re, no usable data on Re concentrations were obtained. Since no more material was available, we rely only on the Os isotopic compositions in this paper.

Composition of mantle xenoliths

The mantle xenoliths from Ubekendt Ejland mainly show coarse and protogranular textures with a few having porphyroclastic texture (classification after

Fig. 1 Simplified map of
Ubekendt Ejland in central
West Greenland. Lavas
generally dip to the west and
the xenolith-bearing upper
lava succession at Eqqua
represents the youngest
volcanic products on the
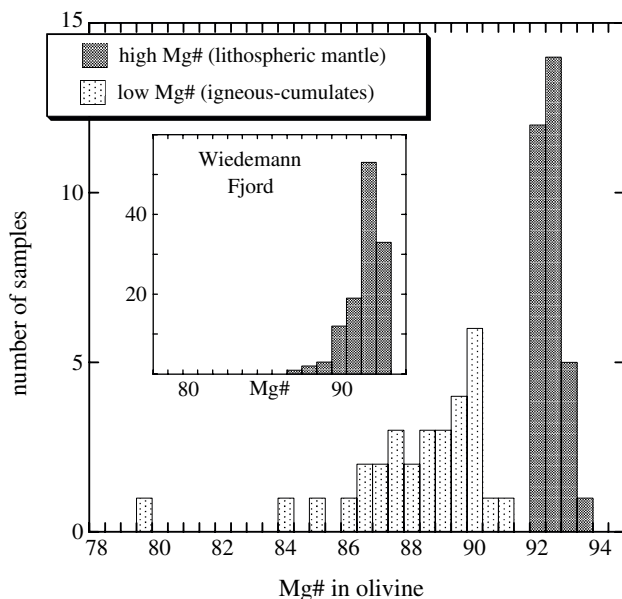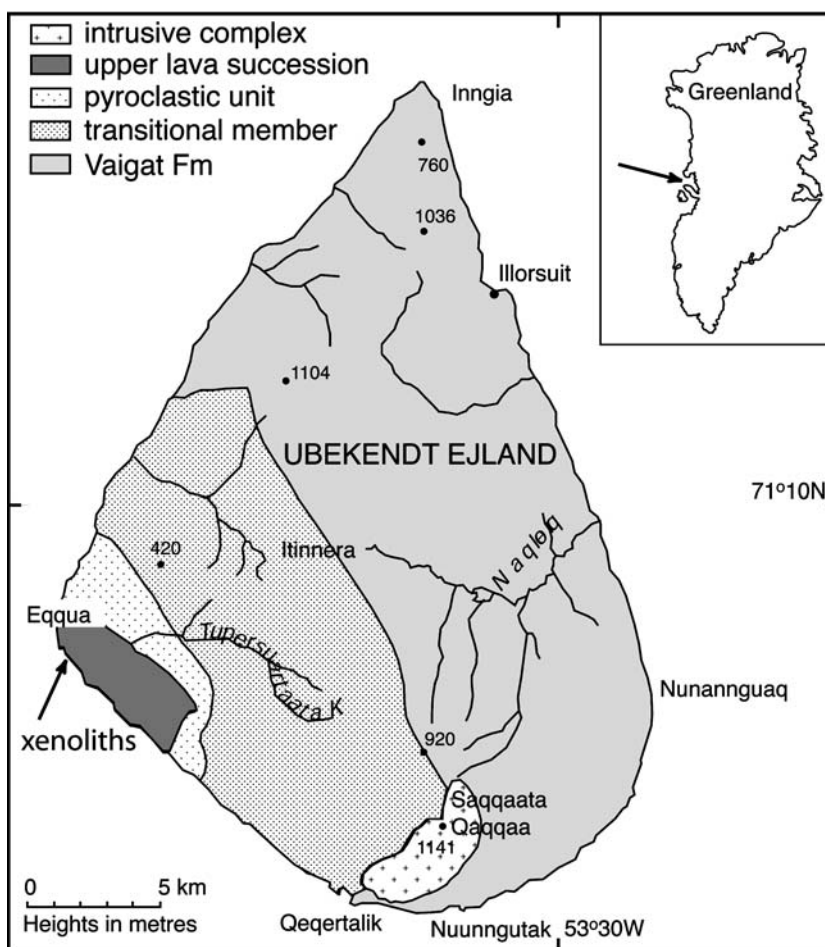island. Map based on Larsen
(1977a, b)

Mercier and Nicolas 1975). Grain size of olivine is
1–4 mm for the protogranular types and >4 mm for
coarse xenoliths. Orthopyroxene occurs as 0.1–1 mm
interstitial grains. Spinel is present in many, but not all,
samples and is opaque with a grain size less than
0.5 mm. No optical or chemical zoning was observed in
any of the minerals.

The Ubekendt Ejland xenoliths have 0–2.8% modal
spinel, 0–9.5% orthopyroxene (Table 1) and corre-
spondingly high olivine contents (90.2–100%). The
high olivine content is a feature they share with the
Wiedemann Fjord xenoliths from East Greenland
(Bernstein et al. 1998). As illustrated in Figs. 2 and 3,
the Ubekendt Ejland xenoliths have olivine composi-
tions similar to those from Wiedemann Fjord with
average Mg# of 92.6 versus 92.7%, respectively. The
modal olivine contents of the Ubekendt Ejland xeno-
liths are somewhat higher than those from Wiedemann
Fjord, which again are higher than modal olivine con-
tents in cratonic xenoliths from Siberia and South
Africa (Fig. 3 and Bernstein et al. 1998). Nickel in
olivine is low, with an average of 2,731 ppm (varies

Fig. 2 Olivine composition in terms of Mg# (= $100 \times Mg/(Mg + Fe)$) for the two populations of xenoliths from Ubekendt
Ejland. Note the compositional gap between the two groups.
Inset shows the olivine compositional distribution of the
Wiedemann Fjord xenolith suite (Bernstein et al. 1998)

Table 1 Modal and mineral chemistry data of peridotite xenoliths from Ubekendt Ejland, West Greenland

Sample ID	452001			452002			452003			452006			452008		452009			452016	
Mineral Mode (vol.%)	ol 92.3	opx 6.3	sp 1.4	ol 96.8	opx 2.1	sp 1.1	ol 93.0	opx 5.8	sp 1.2	ol 91.1	opx 7.6	sp 1.3	ol 98.4	sp 1.6	ol 95.5	opx 3.1	sp 1.4	ol 98.8	sp 1.2
Na_2O	0.03	0.01		0.01	0.01		0.02	0.04		0.02	0.04		0.03		0.02	0.01		0.03	
MgO	51.54	36.18	17.30	51.62	36.80	11.98	52.17	36.35	16.95	51.52	36.86	11.57	50.76	12.15	50.93	36.59	10.92	50.86	11.08
Al_2O_3	0.02	1.46	28.94	0.01	0.09	5.14	0.02	1.69	29.85	0.01	0.07	4.00	0.02	9.87	0.02	0.71	5.07	0.02	2.89
SiO_2	41.69	57.68	0.05	41.67	58.89	0.18	41.39	56.82	0.01	41.24	58.41	0.25	41.19	0.09	41.34	58.77	0.17	40.56	0.18
CaO	0.04	0.16	0.01	0.05	0.11	0.01	0.04	0.27	0.02	0.05	0.18	0.01	0.04	0.02	0.02	0.08	0.02	0.02	0.03
TiO_2	0.01	0.02	0.01	0.06	0.01	0.04	0.01	0.01	0.01	0.01	0.01	0.10	0.02	0.04	0.03	0.01	0.48	0.02	0.11
Cr_2O_3	0.02	0.24	40.80	0.03	0.05	62.44	0.02	0.11	39.43	0.03	0.03	61.35	0.02	54.27	0.02	0.09	60.02	0.02	60.50
MnO	0.07	0.14	0.20	0.13	0.11	0.15	0.09	0.10	0.17	0.07	0.12	0.32	0.11	0.27	0.10	0.26	0.33	0.13	0.37
FeO	7.06	4.67	12.04	7.29	4.86	19.37	7.27	4.59	13.11	7.46	4.75	20.55	7.58	20.64	7.46	4.76	20.91	7.10	20.56
NiO	0.37	0.08	0.18	0.35	0.04	0.12	0.36	0.11	0.15	0.36	0.07	0.07	0.36	0.16	0.34	0.08	0.12	0.31	0.08
Total	100.87	100.65	99.54	101.21	100.97	99.42	101.39	100.11	99.69	100.78	100.54	98.21	100.14	97.50	100.28	101.36	98.03	99.07	95.80
Mg#	92.79	93.05	76.01	92.54	92.94	59.60	92.67	93.21	74.24	92.42	93.08	58.62	92.16	60.63	92.30	92.85	55.19	92.61	58.17
Cr#			48.61			89.07			46.98			91.15		78.68			88.82		93.35
T_1 (°C)	913			923			860			936			901		878			937	
T_2 (°C)	783			660			753			653					698				

Sample ID	452018			452021		452022			452023	452028		455901		455903			455906		455907	
Mineral Mode (vol.%)	ol 90.2	opx 9.1	sp 0.7	ol 98.9	sp 1.1	ol 95.7	opx 1.8	sp 2.5	opx	ol 97.9	sp 0.6	ol 99.7	sp 0.3	ol 98.2	opx 1.0	sp 0.8	ol 98.4	sp 1.6	ol 90.5	opx 9.5
Na_2O	0.02	0.03		0.03		0.02	0.03		0.03	0.03		0.02		0.03	0.02		0.02		0.02	0.03
MgO	51.64	36.82	11.36	51.97	13.31	51.92	36.96	11.42	36.94	51.57	14.22	51.67	13.16	51.00	36.58	12.01	51.09	12.67	50.35	35.52
Al_2O_3	0.01	0.19	8.06	0.02	9.22	0.01	0.10	4.96	0.08	0.02	16.01	0.01	5.98	0.02	0.21	8.55	0.02	13.19	0.06	0.43
SiO_2	41.31	58.25	0.10	41.45	0.16	41.45	58.56	0.12	58.60	41.39	0.15	41.78	1.42	41.78	58.85	0.14	41.89	0.13	41.64	57.59
CaO	0.02	0.10	0.02	0.05	0.02	0.03	0.08	0.02	0.06	0.05	0.04	0.03	0.02	0.04	0.11	0.02	0.02	0.01	0.04	0.11
TiO_2	0.01	0.03	0.17	0.02	0.29	0.02	0.03	0.20	0.04	0.01	0.12	0.01	0.49	0.03	0.03	0.15	0.04	0.10	0.02	0.02
Cr_2O_3	0.01	0.07	58.12	0.02	58.81	0.02	0.07	59.91	0.03	0.02	51.31	0.02	59.62	0.01	0.04	56.62	0.04	55.41	0.04	0.14
MnO	0.11	0.10	0.35	0.08	0.32	0.10	0.18	0.39	0.08	0.13	0.24	0.17	0.36	0.09	0.14	0.23	0.11	0.29	0.12	0.15
FeO	7.05	4.53	19.63	6.96	16.13	7.09	4.69	21.40	4.71	7.79	16.67	6.70	15.28	7.21	4.48	20.16	7.48	17.29	7.58	5.26
NiO	0.37	0.07	0.07	0.37	0.13	0.36	0.06	0.08	0.07	0.38	0.15	0.34	0.12	0.40	0.08	0.18	0.34	0.12	0.37	0.06
Total	100.57	100.18	97.88	100.98	98.37	101.03	100.76	98.52	100.66	101.39	98.92	100.75	96.45	100.59	100.54	98.06	101.03	99.21	100.23	99.30
Mg#	92.77	93.42	57.14	92.94	65.14	92.78	93.11	57.80	93.21	92.06	67.06	93.06	63.37	92.57	93.38	59.75	92.31	61.06	92.10	92.13
Cr#			82.87		81.06			89.01			68.25		87.00			81.62		73.81		
T_1 (°C)	833			939		897				932		937		883			837		708	
T_2 (°C)	671					665			652					658						

Table 1 continued

Sample ID	455910	455910	455916	455916	455916	455918	455918	455918	455920	455920	455920	455921	455921	455923	455923	455927	455927	455930	455930	455930
Mineral	ol	opx	ol	opx	sp	ol	opx	sp	ol	opx	sp	ol	sp	ol	sp	ol	sp	ol	opx	sp
Mode (vol.%)	95.0	5.0	98.0	0.4	1.6	96.0	2.1	1.9	98.3	0.7	1.0	97.2	2.8	100.0	0.6	99.2	0.8	96.8	2.8	0.4
Na_2O	0.02	0.02	0.03	0.03		0.01	0.03		0.01	0.03		0.02		0.02		0.01		0.02	0.03	
MgO	50.98	36.20	50.94	36.01	10.35	51.00	36.22	14.91	51.29	36.54	13.13	50.66	9.53	51.26	10.76	51.11	11.91	51.50	36.45	14.37
Al_2O_3	0.02	0.24	0.02	0.02	1.74	0.02	0.35	20.37	0.02	0.15	8.49	0.02	1.97	0.02	2.19	0.02	4.88	0.02	0.30	17.54
SiO_2	41.62	58.81	41.59	58.66	0.15	41.57	58.86	0.11	41.71	58.96	0.16	41.54	0.20	41.68	0.19	41.07	0.16	41.66	58.52	0.14
CaO	0.02	0.10	0.03	0.07	0.01	0.03	0.14	0.03	0.03	0.13	0.01	0.03	0.01	0.06	0.02	0.03	0.01	0.02	0.10	0.01
TiO_2	0.03	0.01	0.01	0.01	0.13	0.01	0.03	0.12	0.01	0.03	0.03	0.01	0.07	0.01	0.12	0.03	0.19	0.03	0.02	0.22
Cr_2O_3	0.02	0.04	0.02	0.11	63.78	0.03	0.01	46.43	0.05	0.04	59.16	0.01	63.80	0.04	62.92	0.03	63.70	0.02	0.06	48.61
MnO	0.12	0.11	0.14	0.14	0.32	0.13	0.12	0.18	0.11	0.12	0.23	0.11	0.22	0.15	0.28	0.14	0.33	0.14	0.10	0.21
FeO	7.76	5.20	7.64	5.03	22.25	7.46	4.60	16.08	7.01	4.42	17.17	7.68	22.81	6.94	21.32	6.70	17.10	6.42	4.31	17.17
NiO	0.36	0.06	0.34	0.06	0.07	0.37	0.09	0.14	0.34	0.10	0.06	0.36	0.10	0.32	0.09	0.34	0.09	0.37	0.06	0.13
Total	100.96	100.79	100.75	100.13	98.79	100.63	100.45	98.37	100.58	100.50	98.44	100.45	98.70	100.48	97.88	99.36	98.37	100.20	99.95	98.41
Mg#	92.01	92.39	92.11	92.55	53.33	92.30	93.19	69.04	92.77	93.49	64.58	92.05	49.26	92.81	55.54	93.13	60.07	93.33	93.65	67.30
Cr#					96.09			60.46			82.38		95.59		95.06		89.75			65.02
T_1 (°C)	662		902			897			947			839				896		847		
T_2 (°C)			678			656			659									672		

Sample ID	455931	455931	455932	455932	455932	455934	455934	455942	455942	455942	455943	455943	455948	455948	455948	455954	455954	455954
Mineral	ol	sp	ol	opx	sp	ol	sp	ol	opx	sp	ol	sp	ol	opx	sp	ol	opx	sp
Mode (vol.%)	97.8	2.2	98.1	0.4	1.9	99.0	1.0	96.6	2.0	1.4	99.5	0.5	99.0	0.4	0.6	97.4	1.6	0.8
Na_2O	0.02		0.02			0.02		0.02	0.02		0.02		0.02	0.02		0.02	0.04	
MgO	50.39	10.05	51.30		11.89	50.84	12.78	51.15	36.53	12.52	51.39	12.93	51.83	36.97		51.17	36.49	11.10
Al_2O_3	0.02	1.87	0.02		3.91	0.01	13.64	0.01	0.17	10.72	0.01	6.35	0.01	0.05		0.02	0.08	2.97
SiO_2	40.85	0.42	40.97		0.21	41.18	0.09	40.99	58.03	0.20	41.29	0.14	41.43	58.49		41.24	58.57	0.10
CaO	0.03	0.02	0.03		0.01	0.04	0.02	0.02	0.11	0.39	0.03	0.02	0.02	0.06		0.04	0.14	0.03
TiO_2	0.01	0.13	0.01		0.31	0.03	0.14	0.03	0.03	0.13	0.01	0.04	0.04	0.05		0.02	0.04	0.22
Cr_2O_3	0.03	61.64	0.02		64.42	0.02	54.19	0.02	0.04	56.67	0.04	62.98	0.02	0.03		0.07	0.07	61.81
MnO	0.08	0.24	0.18		0.20	0.15	0.26	0.08	0.13	0.37	0.13	0.13	0.11	0.08		0.09	0.09	0.24
FeO	7.43	23.00	6.39		16.51	7.37	17.32	6.36	4.26	17.08	7.02	16.38	6.07	4.03		7.12	4.57	21.86
NiO	0.36	0.10	0.28		0.05	0.31	0.10	0.33	0.07	0.10	0.33	0.07	0.32	0.07		0.35	0.08	0.09
Total	99.21	97.46	99.21		97.51	99.96	98.53	99.01	99.37	98.19	100.26	99.04	99.85	99.85		100.06	100.16	98.42
Mg#	92.28	51.87	93.30		60.18	92.34	61.74	93.40	93.69	62.27	92.76	63.85	93.73	94.13		92.70	93.32	56.66
Cr#		95.68			91.70		72.72			78.01		86.94						93.32
T_1 (°C)	873		902			843		838			960		848			913		
T_2 (°C)								658					648			666		

T_1 is olivine–spinel thermometer (Ballhaus et al. 1991); T_2 is Cr-Al-in-orthopyroxene (Witt-Eickschen and Seck 1991); Mg# = $100 \times Mg/(Mg + Fe)$; Cr# = $100 \times Cr/(Cr + Al)$

ol olivine, *opx* orthopyroxene, *sp* spinel

Table 2 Osmium isotopic composition of mineral separates from Ubekendt Ejland peridotite xenoliths

Sample	Phase	Os (pg/g)	$^{187}Os/^{188}Os$	2 SE (absolute)	Trd (Ma)
452001	Olivine	1,067	0.1233	0.00031	549
452001	Spinel	11,027	0.1336	0.00055	– 992
452002	Olivine	1,431	0.1046	0.00037	3,275
452002	Spinel	30,075	0.1080	0.00078	2,789
452003	Olivine	5,28	0.1141	0.00113	1,900
452028	Olivine	400	0.1194	0.00147	1,125
455903	Olivine	1,874	0.1099	0.00179	2,512
452008	Spinel	15,426	0.1061	0.00146	3,049
452114	Spinel	6,945	0.1309	0.00051	– 593
455918	Spinel	15,124	0.1155	0.00055	1,694

Trd = rhenium-depletion ages, calculated with respect to chondritic evolution, including $^{187}Re/^{188}Os = 0.40186$ (Shirey and Walker 1998) and $^{187}Os/^{188}Os = 0.127$ (Shirey and Walker 1998)

from 2,187 to 3,023 ppm). This is slightly, but significantly, lower than Ni in olivine in the Wiedemann Fjord xenoliths, which averages 2,865 ppm and ranges from 2,148 to 3,349 ppm (Kelemen et al. 1998).

Orthopyroxene is found in 18 of 31 dunite samples and has very low contents of aluminium, calcium and chromium. Al_2O_3 is between 0.024 and 0.713 wt%, except for two samples (452001 and 452003), which have 1.463 and 1.693 wt% Al_2O_3, respectively. CaO varies between 0.062 and 0.275 wt% and Cr_2O_3 between 0.013 and 0.236 wt%, with the high end of the ranges defined by the two samples 452001 and 452003.
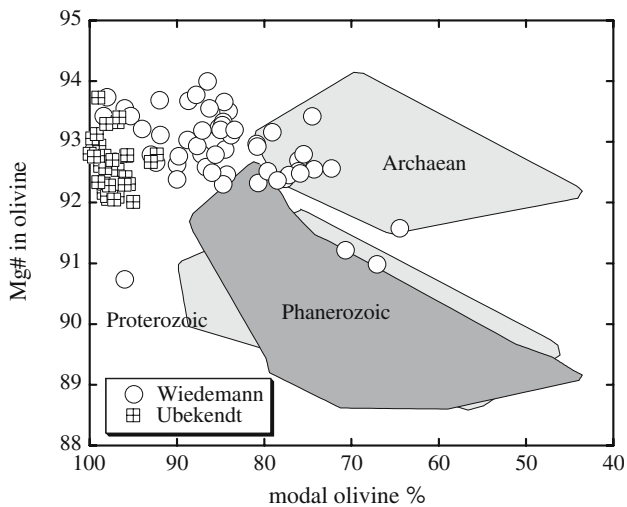
Fig. 3 Mg# in olivine versus modal composition of the Ubekendt Ejland mantle xenoliths expressed as vol.% olivine. Also shown are data from the highly depleted Wiedemann Fjord xenoliths in Tertiary East Greenland (Bernstein et al. 1998) and compositional fields for mantle peridotite from Archaean cratons (xenoliths) and mantle peridotite of Proterozoic and Phanerozoic origins, comprising xenoliths, orogenic massifs, ophiolites and abyssal peridotites (Boyd 1989; Menzies 1990)

Figure 4 illustrates the relationship between Al_2O_3 in orthopyroxene and modal olivine content. Most samples cluster at >95% olivine and <0.5 wt% Al_2O_3 in orthopyroxene, and there is a weak negative correlation between these parameters. The data from Ubekendt Ejland and Wiedemann Fjord xenoliths define an array of overall negative correlation, with the Ubekendt Ejland xenoliths defining the refractory end of the array. There is only slight overlap between the two localities. The aluminium content of orthopyroxene from Ubekendt Ejland xenoliths is lower than recorded in most other spinel-bearing xenoliths of mantle origin. For spinel peridotites, Al_2O_3 in orthopyroxene is typically between 0.5 and 4 wt% (e.g. Boyd et al. 1999; Rudnick et al. 1994; Kopylova and Caro 2004). Orthopyroxene may attain Al_2O_3 contents less than 0.1 wt% when equilibrated with chlorite before recrystallization and dehydration of chlorite-bearing peridotites (e.g. Smith and Riter 1997) or when formed during reaction between peridotite and hydrous fluids (e.g. Morishita et al. 2003). Such origins for the low-Al orthopyroxenes of the Ubekendt Ejland xenoliths are unlikely because of the lack of chlorite, the homogeneous nature of the orthopyroxene grains and the absence of high-Al orthopyroxene in addition to low-Al orthopyroxene. It is most likely that the low Al_2O_3 contents reflect the low equilibrium temperature at which aluminous and chromian pyroxene components + olivine break down to enstatite + spinel (e.g. Witt-Eickschen and Seck 1991).

Spinel has Cr# (= $100 \times Cr/(Cr + Al)$) between 60.55 and 95.67 for all but two samples. Again samples
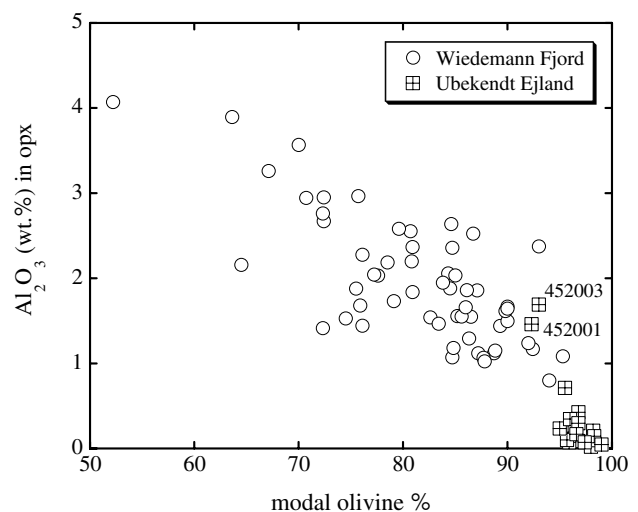

Fig. 4 Weight percent Al_2O_3 in orthopyroxene versus modal olivine (vol.%) in mantle xenoliths from Ubekendt Ejland and Wiedemann Fjord (Bernstein et al. 1998). Sample numbers are given for two aberrant Ubekendt Ejland samples

452001 and 452003 differ in composition from the rest of the samples, having lower Cr# of 48.63 and 46.98, respectively. In the Ubekendt Ejland data alone, there is a weak correlation between modal olivine contents and Cr# in spinel (Fig. 5). Ubekendt Ejland and Wiedemann Fjord xenoliths together define an overall positive correlation in Fig. 5. In terms of the spinel Mg#–Cr# compositions (Fig. 6a), the Ubekendt Ejland xenoliths plot as a continuation of the Wiedemann Fjord xenoliths and roughly follow the trend of data for other cratonic spinel-harzburgites (Hervig et al. 1980). A similar relationship can be seen in Fig. 6b, with Cr# in spinel versus Mg# of coexisting olivine. The Ubekendt Ejland xenoliths form a nearly vertical trend, with little variation in olivine Mg# for a large variation in spinel Cr#, roughly parallel to the pattern defined by the kimberlite-hosted spinel harzburgites reported by Hervig et al. (1980).

Equilibrium temperatures

Temperatures have been calculated on the basis of orthopyroxene chemistry, using Cr and Al (Witt-Eickschen and Seck 1991), and spinel–olivine chemistry, using Fe–Mg exchange after Ballhaus et al. (1991). The widely used Ca-in-opx thermometer (Brey and Köhler 1990), based on Ca exchange between orthopyroxene and clinopyroxene, cannot be used as clinopyroxene is not present in the samples chosen for this study.

The Cr-Al–opx geothermometer is based on Cr–Al exchange between orthopyroxene and spinel, which
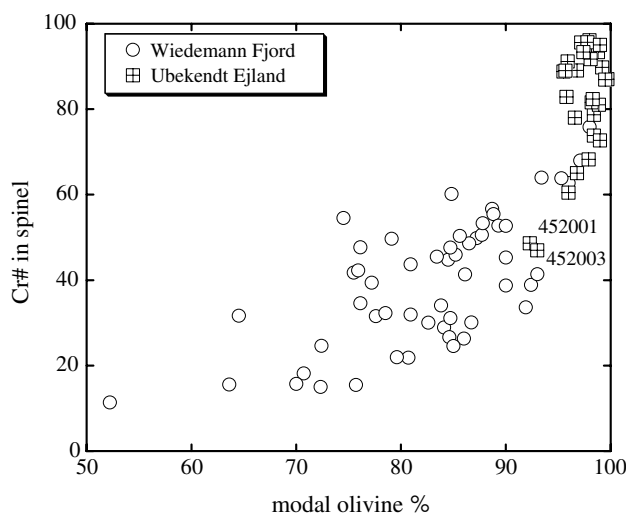
are commonly found in the same samples. Equilibrium temperatures for Ubekendt Ejland xenoliths fall in the range 648–783°C, with most samples in the interval 648–700°C (Fig. 7). Two samples (452001 and 452003, the aberrant samples in Figs. 4, 5) yield temperatures of 783 and 753°C, respectively. Omitting these two outliers, the temperature range for most samples is lower than the Cr-Al-opx temperatures for the Wiedemann Fjord xenoliths (Bernstein et al. 1998) by nearly 200°C, and it places the Ubekendt Ejland xenoliths close to a model conductive geotherm at 2–2.5 GPa (60–75 km depth) using a surface heat flow of 44 mW/m^2 (Pollack and Chapman 1977). The two samples showing elevated temperatures are more similar to the Wiedemann Fjord xenoliths. If these two samples equilibrated along a cratonic conductive geotherm, outlined above, the temperatures would correspond to depths of nearly 100 km, well within the garnet stability field. Because of the highly refractory nature of the Ubekendt Ejland xenoliths, we have no means of constraining their actual depth of equilibration. However, erupted picritic and basaltic lavas on Ubekendt Ejland, and elsewhere in central West Greenland in the early Palaeogene, show that polybaric decompression melting of the mantle proceeded into the spinel lherzolite stability field (e.g. Holm et al.
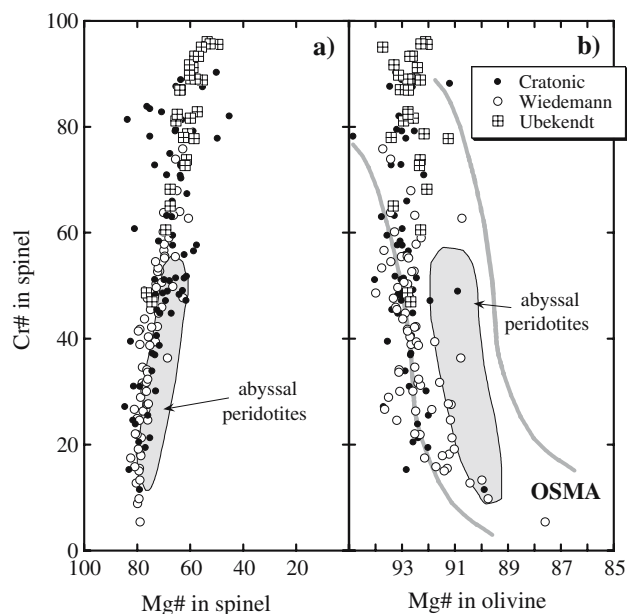
Fig. 6 Spinel compositions in terms of Cr# and Mg# (**a**) and Cr# in spinel versus Mg# of coexisting olivine (**b**). The compositional field for abyssal peridotites is from Dick and Bullen (1984), and the *filled circles*, representing spinel peridotites from cratonic settings, are from Hervig et al. (1980). Data for Wiedemann Fjord xenoliths are from Bernstein et al. (1998). The *field between the two grey lines* is the olivine–spinel mantle array OSMA (Arai 1994)

Fig. 5 Cr# (= $100 \times \text{Cr}/(\text{Cr} + \text{Al})$) in spinel versus modal olivine (in vol.%) for mantle xenoliths from Ubekendt Ejland and Wiedemann Fjord (Bernstein et al. 1998)
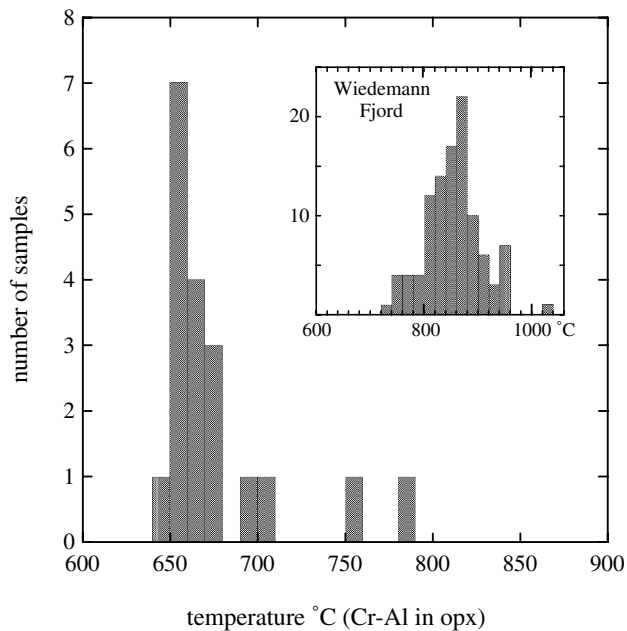
Fig. 7 Distribution of calculated temperatures for the Ubekendt Ejland mantle xenoliths based on orthopyroxene–spinel equilibria (Witt-Eickschen and Seck 1991). Inset shows distribution of calculated temperatures of the Wiedemann Fjord xenoliths (Bernstein et al. 1998)

Fig. 8 Calculated equilibrium temperatures for mantle xenoliths from Ubekendt Ejland and Wiedemann Fjord: $T_{Cr-Al-opx}$ from Witt-Eickschen and Seck (1991), while the y-axis temperature is based on Fe–Mg exchange (T_{ol-sp}) between olivine and spinel (Ballhaus et al. 1991)

1993). Thus, temperatures must have been greater than ~ 1,350°C at depths of 100 km at this time, and active mantle upwelling must have extended to shallower depths. As a result, it seems unlikely that ancient cratonic mantle could have been preserved at these depths. Instead, it is more probable that samples 452001 and 452003 were derived from the same depth interval as the other Ubekendt Ejland xenoliths, but were reheated slightly during Palaeogene magmatism.

Equilibrium temperatures obtained by the Fe–Mg exchange between olivine and spinel (Ballhaus et al. 1991) fall in the range 833–960°C. The data from the two thermometers for Ubekendt Ejland and Wiedemann Fjord xenoliths are summarized in Fig. 8. While the two independent thermometers yield approximately similar temperature ranges for the Wiedemann Fjord xenoliths, the olivine–spinel thermometer generally yields temperature estimates 200–250°C higher than the Cr-Al-orthopyroxene thermometer for the Ubekendt Ejland xenoliths. One explanation for this discrepancy is that the higher olivine–spinel equilibrium temperatures reflect a recent heating event, perhaps during the Palaeogene continental rifting and only a short time prior to the sampling of the xenoliths by the alkaline basaltic melts. Because of the considerably higher diffusion rates of Fe–Mg exchange between olivine and spinel compared to the reaction
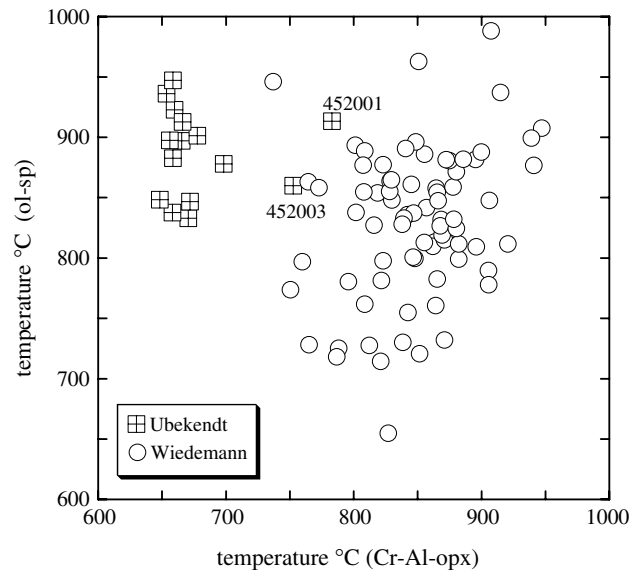
enstatite + spinel to Mg-tschermaks + olivine (Freer 1981), upon which the Cr-Al-orthopyroxene thermometer is based, the olivine–spinel thermometer can react more swiftly to a regional temperature change. Also, in the Ubekendt Ejland xenoliths, spinel is everywhere in contact with olivine, so the diffusion length for the Fe–Mg exchange is much smaller than for the Cr–Al exchange between orthopyroxene and spinel, which are rarely in contact with one another

Os isotopic composition

The Os isotopic composition of the mineral separates from the Ubekendt Ejland xenoliths correlates with modal olivine, aluminium in orthopyroxene and Cr# in spinel, as illustrated in Figs. 9 and 10. Qualitatively, the Ubekendt Ejland data resemble Os isotope data for the Wiedemann Fjord xenoliths (Hanghøj et al. 2000), but are displaced towards higher modal olivine, higher Cr# in spinel and lower Al_2O_3 in orthopyroxene, reflecting the main compositional differences between the two xenolith suites outlined above. For Ubekendt Ejland alone, the relationship between modal olivine and osmium isotopic composition is shown in Fig. 9b. Within this narrow compositional range of 90–100% modal olivine, there is a weak negative correlation, so that samples with the highest proportion of olivine tend to have the lowest Os isotope ratio.

Fig. 9 Os isotopic composition of olivine and spinel separates from **a** Ubekendt Ejland and Wiedemann Fjord xenoliths (Wiedemann Fjord data from Hanghøj et al. 2000) and **b** from Ubekendt Ejland only. The *symbols connected by tie lines* in **b** represent olivine and spinel separates from same sample
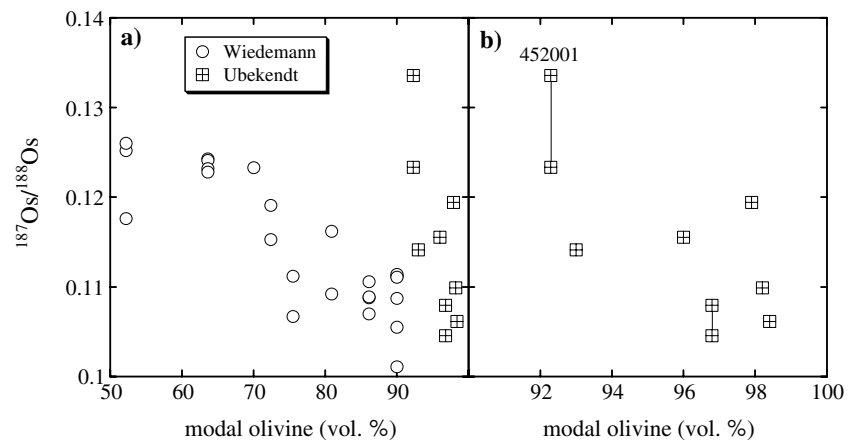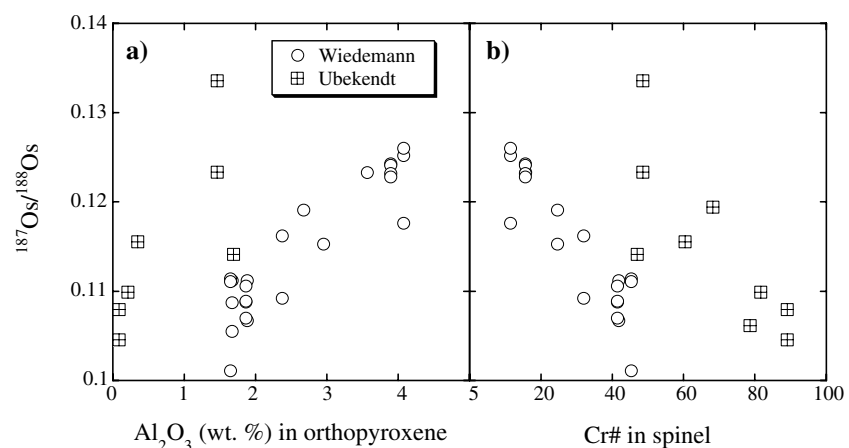

Fig. 10 Os isotopic composition of olivine and spinel separates from Ubekendt Ejland and Wiedemann Fjord xenoliths (data source as in Fig. 9) against Al_2O_3 in orthopyroxene (**a**) and Cr# in spinel (**b**)

For the Wiedemann Fjord xenolith suite, Hanghøj et al. (2000) demonstrated that lherzolites consistently have more radiogenic Os compared to harzburgites. This led to the conclusion that the harzburgites with unradiogenic Os isotopes (yielding Archaean Re-depletion ages) originated as residues from melt extraction and consequently Re depletion in the Archaean. The Wiedemann Fjord lherzolites with relatively radiogenic Os isotopic compositions ($^{187}Os/^{188}Os > 0.115$; Fig. 9a) were considered to have an origin similar to the harzburgites, but with subsequent modal metasomatism (Hanghøj et al. 2000). We reached this conclusion because bulk CaO in some lherzolite xenoliths is higher than in estimates for primitive mantle. This rules out an origin for the lherzolites as restites from relatively low degrees of mantle melting. Such metasomatism probably introduced Re, and possibly also radiogenic Os, which over time resulted in the radiogenic Os isotopic values for the lherzolites.

For the Ubekendt Ejland xenoliths, the range in $^{187}Os/^{188}Os$ values is similar to that of the Wiedemann Fjord xenoliths. This is somewhat surprising, because

all Ubekendt Ejland xenoliths are refractory with modal olivine > 90% (Fig. 9). The correlations between mode and mineral chemistry and $^{187}Os/^{188}Os$ for the Ubekendt Ejland xenoliths (Figs. 9, 10) can be interpreted in two ways. Either (1) they represent metasomatism superimposed on the original depleted residues, as proposed for the Wiedemann Fjord xenoliths by Hanghøj et al. (2000) or (2) they reflect the time-integrated result of variable Re depletion. Such variable Re depletion could stem from incomplete melt extraction, leaving small volumes of melt with higher Re/Os and higher Al/Cr than the solid restite that, with time, developed elevated $^{187}Os/^{188}Os$. The present data set does not allow for a detailed discussion of these possibilities.

Ubekendt Ejland and Wiedemann Fjord xenoliths suites and mantle melting

In several respects, the Ubekendt Ejland xenoliths resemble the mantle xenolith suite from Wiedemann Fjord in East Greenland. Both groups have highly

magnesian olivines (average Mg# of 92.6 and 92.7, respectively—see Fig. 2), and low modal orthopyroxene (< 10 and < 20 vol.%, respectively; Table 1 and Bernstein et al. 1998). Using simple mass balance calculations, Bernstein et al. (1998) estimated the Wiedemann Fjord xenoliths to represent restites after 38–40% melt extraction from mantle peridotite, depending on the choice of mantle peridotite protolith, either pyrolite (Ringwood 1966) or Hart and Zindler's (1986) primitive mantle, respectively. The melting was envisaged to take place in upwelling mantle starting at about 7 GPa and ending at low pressures <2 GPa (Bernstein et al. 1998). The highly refractory nature of the Ubekendt Ejland xenoliths suggests that they too formed as restites from high-degree partial melting of mantle peridotite. Using the mass-balance technique of Bernstein et al. (1998) for the average Ubekendt Ejland xenolith composition suggests that they are restites after 39–41% melt extraction.

Although the major element compositions and Mg# of the two xenolith suites thus appear to reflect similar degrees of melt extraction, there are some fundamental differences between the two xenolith populations that need to be addressed. Ubekendt Ejland xenoliths have a higher average modal olivine content (Fig. 3) and higher Cr# in spinel at a given olivine composition (Fig. 6b) compared to the Wiedemann Fjord xenoliths. Also, the aluminium content in orthopyroxene is distinctly lower than in Wiedemann Fjord xenoliths (Fig. 4). There may be several explanations for these differences:

1. The Wiedemann Fjord xenoliths with their slightly higher modal orthopyroxene are products of modest melt/rock reaction between a protolith, like that of the Ubekendt Ejland dunite xenoliths, and silica-rich melts from subducted basalts, or eclogites, as proposed by Kelemen et al. (1998) for the formation of orthopyroxene-rich harzburgites of the Kaapvaal and Siberian cratons. However, this process alone probably cannot explain the lower Cr# in Wiedemann Fjord spinels.

2. The average pressure of mantle melting was higher for Ubekendt Ejland xenolith suite, leading to exhaustion of garnet during melting. This would drive up the Cr# in the residue since no Al-bearing phase (other than Tschermak's component in pyroxenes) was present to retain Al in the residue. For the Wiedemann Fjord xenolith suite, due to a somewhat lower average pressure of melting, residual garnet may have persisted until the upwelling residue entered the spinel stability field,

thereby maintaining a relatively high Al content in orthopyroxene and low Cr# in spinel.

3. Hanghøj et al. (2002) tentatively suggested that both xenolith suites represent restites from advanced degrees of partial melting, but the Ubekendt Ejland xenolith suite underwent melting under hydrous conditions, perhaps in the forearc of an Archaean subduction zone environment. One of the main arguments for an arc-related origin is the high Cr# (> 50) of spinel in Ubekendt Ejland xenoliths, similar to that found in spinel from depleted mantle peridotites from present-day arc settings (e.g. Arai 1994).

As discussed below, we find that hypothesis 3 is less likely, and instead favour some combination of 1 and 2, i.e. higher average pressure of melting for Ubekendt Ejland xenoliths and perhaps some degree of melt–rock reaction for Wiedemann Fjord xenoliths, to explain the higher modal orthopyroxene contents at same olivine Mg# in Wiedemann compared to Ubekendt xenoliths.

Did shallow cratonic mantle form in arcs?

Available data show that arc-related mantle peridotite differs in some aspects from the Wiedemann Fjord and Ubekendt Ejland xenolith suites. In terms of Cr# and Mg# of spinel, the Ubekendt Ejland–Wiedemann Fjord data form a steeper trend, compared to that for peridotites from arc and mid-ocean ridge settings (Fig. 11a). The Mg# of spinel is controlled mainly by temperature-dependent Fe–Mg exchange with olivine, and the difference between the cratonic and arc trends in Fig. 11a is thus explained—at least in part—by the higher olivine–spinel equilibration temperatures for the cratonic xenoliths (on average about 900°C) compared to temperatures of arc-related and abyssal peridotite samples which mostly lie in the 600–650°C range (Dick and Bullen 1984; Dick 1989; Parkinson and Pearce 1998; Kubo 2002).

Another way in which the Ubekendt Ejland–Wiedemann Fjord xenolith suites differ from the arc peridotite trend, that is not dependent on subsolidus equilibration, is presented in Fig. 11b. Arc peridotites extend the data array defined by abyssal peridotites to higher Cr# in spinel and Mg# in olivine, well within the olivine–spinel mantle array of Arai (1994). In contrast, the Ubekendt Ejland–Wiedemann Fjord data form a continuous, steep trend along the low Cr#–high Mg# edge of the olivine–spinel mantle array (Fig. 11b), as
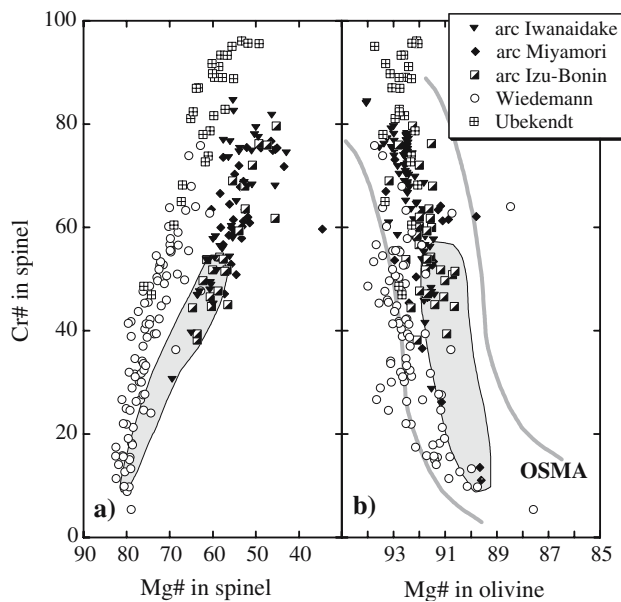
Fig. 11 Variations in spinel Cr# versus spinel Mg# (**a**) and versus Mg# in olivine (**b**) for the Wiedemann Fjord–Ubekendt Ejland xenolith suites, shown together with data for abyssal peridotites and arc-related peridotites. Data sources: Iwanaidake, Japan: Kubo (2002); Miyamori, Japan: Ozawa (1994); Ozawa and Shimizu (1995); Izu-Bonin: Parkinson and Pearce (1998); abyssal peridotites: Dick and Bullen (1984). The *field between the two grey lines* is the olivine–spinel mantle array OSMA (Arai 1994)

Fig. 12 Cr# in spinel versus modal olivine in volume percent. The data from Wiedemann Fjord and Ubekendt Ejland extend the data array from abyssal peridotites towards dunites with spinel of Cr# 60–97. The data array formed by peridotites from arc settings is distinctly different and extends towards dunite with spinel Cr# of 60–85. Data sources for arc-peridotites as in Fig. 11. Spinel peridotite data from Kaapvaal: Hervig et al. (1980) and Boyd et al. (1999); from Tanzania: Lee and Rudnick (1999)

for other cratonic xenoliths from the spinel stability field (Fig. 6; Hervig et al. 1980; see also Bernstein et al. 1998).

Finally, the Ubekendt Ejland–Wiedemann Fjord data form a strongly *concave*-upward trend in a diagram of Cr# in spinel versus modal olivine, whereas the arc-related peridotites display a *convex*-upward trend, and the arc trend lies at higher Cr# for a given proportion of olivine compared to the cratonic mantle xenoliths (Fig. 12). The Ubekendt Ejland–Wiedemann Fjord data appear to extend the abyssal peridotite data field, while the arc-related peridotites follow a very different trend. There is substantial evidence that the "arc" trends in Figs. 11b and 12 represent the result of progressive "fluxed melting" of mantle peridotite above a subduction zone (e.g. Bloomer and Fisher 1987; Ozawa 1988, 1994; Parkinson and Pearce 1998; Abe et al. 1999; Kubo 2002; Ohara et al. 2002).

Experiments on melting of mantle peridotite show that under hydrous conditions the Cr# of residual spinel is elevated compared to that of residual spinel produced under anhydrous melting (Matsukage and Kubo 2003). Therefore, one simple way of interpreting the contrasting trends in Figs. 11b and 12 is that arc and cratonic mantle peridotites both represent the residues of progressive partial melting, in which the
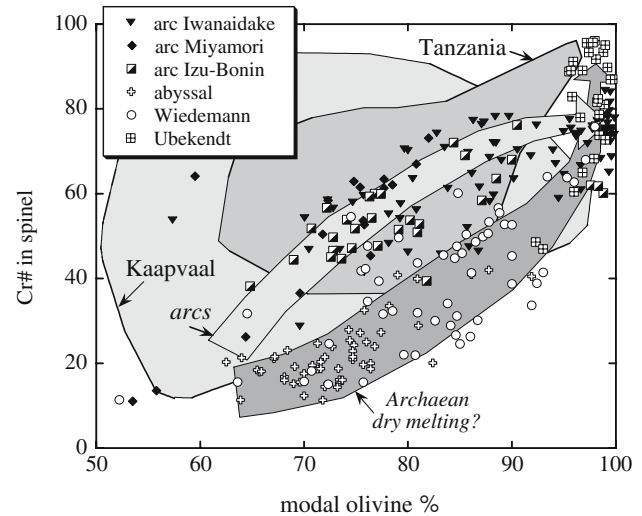
"arc" trend is produced under hydrous conditions whereas the "abyssal-cratonic" trend reflects melting under relatively dry conditions.

Spinel-peridotite xenoliths from other cratons, such as Kaapvaal and Tanzania, have lower modal olivine and higher modal orthopyroxene for a given Cr# in spinel (Fig. 12) or Mg# in olivine (not shown). Considering the rather restricted variations in the "arc" trend depicted in Fig. 12, these orthopyroxene-rich, cratonic peridotites are unlikely to have formed by hydrous melting in arc-settings. Indeed, as mentioned above, such enrichment in orthopyroxene in mantle xenoliths from Kaapvaal and other cratonic areas has been attributed to reaction between an orthopyroxene-poor, high-Mg# restite and silica-rich melts in a subduction zone environment (e.g. Kelemen et al. 1998; Walter 2003). The protolith, prior to the orthopyroxene-forming reaction, is envisaged to be similar to the orthopyroxene-poor mantle xenoliths from Wiedemann Fjord and Ubekendt Ejland.

We conclude that Ubekendt Ejland dunite xenoliths with their refractory compositions and unradiogenic Os isotopes represent residues of extensive partial melting and melt extraction in the Archaean, perhaps reflecting a slightly higher degree of melting than the Wiedemann Fjord xenoliths. The main differences between the two Greenlandic xenolith suites: higher Cr# in spinel, lower Al in orthopyroxene and lower modal orthopyroxene in

the Ubekendt Ejland xenoliths compared to the Wiedemann Fjord xenoliths, can reflect a combination of higher average pressures of melting for the Ubekendt Ejland xenoliths and modest reaction between dunite residue and silica-rich melts for the Wiedemann Fjord xenoliths. Finally, the combined data on shallow lithospheric mantle beneath East and West Greenland and abyssal peridotites differ markedly from trends defined by peridotites from arcs. We thus propose that extensive mantle melting in the early Archaean reflects high potential temperatures in the mantle, rather than melting in subduction zone environments.

References

Abe N, Arai S, Yurimoto H (1999) Texture-dependent geochemical variations of sub-arc mantle peridotite from Japan island arcs. In: Proceedings of the 7th international kimberlite conference on Red Roof Design, Cape Town, pp 13–22

Arai S (1994) Characterization of spinel peridotites by olivine–spinel compositional relationships: review and interpretation. Chem Geol 113:191–204

Ballhaus C, Berry RF, Green DH (1991) High pressure experimental calibration of the olivine–orthopyroxene–spinel oxygen barometer: implications for the oxidation state of the mantle. Contrib Mineral Petrol 107:27–40

Bernstein S, Brooks CK (1999) Mantle xenoliths from Tertiary lavas and dykes at Ubekendt Ejland, West Greenland. Geol Greenl Surv Bull 180:152–154

Bernstein S, Kelemen PB, Brooks CK (1998) Depleted spinel harzburgite xenoliths in Tertiary dykes from East Greenland: restites from high degree melting. Earth Planet Sci Lett 154:221–235

Bizzarro M, Stevenson RK (2003) Major element composition of the lithospheric mantle under the North Atlantic craton: evidence from peridotite xenoliths of the Sarfartoq area, southwestern Greenland. Contrib Mineral Petrol 146:223–240

Bloomer SH, Fisher RL (1987) Petrology and geochemistry of igneous rocks from the Tonga Trench—a nonaccreting plate boundary. J Geol 95:469–495

Boyd FR (1989) Compositional distinction between oceanic and cratonic lithosphere. Earth Planet Sci Lett 96:15–26

Boyd FR, Canil D (1997) Peridotite xenoliths from the Slave craton, Northwest Territories. In: Seventh annual V M Goldschmidt conference. LPI contribution no. 921. Lunar and Planetary Institute, Houston, pp 34–35

Boyd FR, Mertzman SA (1987) Composition and structure of the Kaapvaal lithosphere, southern Africa. In: Mysen BA (ed) Magmatic processes: physiochemical principles. The Geochemical Society, University Park, pp 13–24

Boyd FR, Pearson DG, Mertzman SA (1999) Spinel-facies peridotites from the Kaapvaal Root. In: Proceedings of the 7th international kimberlite conference on Red Roof Design, Cape Town, pp 40–47

Brey GP, Köhler T (1990) Geothermobarometry in four-phase lherzolites II. New thermobarometers, and the practical assessment of existing thermobarometers. J Petrol 31(6):1353–1378

Clarke DB (1973) New mapping in the western part of Ubekendt Ejland. Greenl Geol Surv Rep 53:5–9

Dick HJB (1989) Abyssal peridotites, very slow spreading ridges and ocean ridge magmatism. In: Saunders AD, Norry MJ (eds) Magmatism in the Ocean Basins. Geol Soc Spec Publ 42:71–105

Dick HJB, Bullen T (1984) Chromian spinel as a petrogenetic indicator in abyssal and alpine-type peridotites and spatially associated lavas. Contrib Mineral Petrol 86:54–76

Drever HI, Game PM (1948) The geology of Ubekendt Ejland, West Greenland. Medd Grønl 134:1–34

Freer R (1981) Diffusion in silicate minerals and glasses: a data digest and guide to the literature. Contrib Mineral Petrol 76:440–454

Hanghøj K, Kelemen PB, Bernstein S, Blusztajn J, Frei R (2000) Osmium isotopes in the Wiedemann Fjord mantle xenoliths, a unique record of cratonic mantle formation by melt depletion in the Archaean. Geochem Geophys Geosyst 2:2000GC000085

Hanghøj K, Bernstein S, Kelemen PB, Brooks CK (2002) New evidence for ultra depleted Archaean mantle peridotite beneath Tertiary West Greenland. EOS 81:F1273

Hart SR, Zindler A (1986) In search of a bulk-earth composition. Chem Geol 57:247–267

Hervig RL, Smith JV, Steele IM, Dawson JB (1980) Fertile and barren Al-Cr-spinel harzburgites from the upper mantle: ion and electron probe analyses of trace elements in olivine and orthopyroxene: relation to lherzolites. Earth Planet Sci Lett 50:41–58

Herzberg C (2004) Geodynamic information in peridotite petrology. J Petrol 45:2507–2530

Holm PM, Gill RCO, Pedersen AK, Larsen JG, Hald N, Nielsen TFD, Thirlwall MF (1993) The Tertiary picrites of West Greenland: contributions from 'Icelandic' and other sources. Earth Planet Sci Lett 115:227–244

Kelemen PB, Hart SR, Bernstein S (1998) Silica enrichment in the continental lithosphere via melt/rock reaction. Earth Planet Sci Lett 164:387–406

Kopylova MG, Caro G (2004) Mantle xenoliths from the Southeastern Slave Craton: evidence for chemical zonation in a thick, cold lithosphere. J Petrol 45(5):1045–1067

Kopylova MG, Russell JK, Cookenboo H (1999) Petrology of peridotite and pyroxenite xenoliths from the Jericho kimberlite: implications for the thermal state of the mantle beneath the Slave craton, Northern Canada. J Petrol 40:79–104

Kubo K (2002) Dunite formation processes in highly depleted peridotite: a case study of the Iwanaidake Peridotite, Hakkaido, Japan. J Petrol 43:423–448

Larsen JG (1977a) Fieldwork on Ubekendt Ejland in the Tertiary basalt province of West Greenland, 1971 and 1973. Greenl Geol Surv Rep 79:35–44

Larsen JG (1977b) Transition from low potassium olivine tholeiites to alkali basalts on Ubekendt Ejland. Medd Grønl 200:1–42

Larsen JG (1982) Mantle-derived dunite and lherzolite nodules from Ubekendt Ejland, west Greenland Tertiary province. Mineral Mag 46:329–336

Lee C-T, Rudnick RL (1999) Compositionally stratified cratonic lithosphere: petrology and geochemistry of peridotite xenoliths from the Labait Volcano, Tanzania. In: Proceedings of the 7th international kimberlite conference on Red Roof Design, Cape Town, pp 503–521

Matsukage KN, Kubo K (2003) Chromian spinel during melting experiments of dry peridotite (KLB-1) at 1.0–2.5 GPa. Am Mineral 88:1271–1278

Menzies MA (1990) Archaean, Proterozoic, and Phanerozoic lithosphere. In: Menzies MA (ed) Continental mantle. Oxford University Press, Oxford, pp 67–86

Mercier J-CC, Nicolas A (1975) Textures and fabrics of upper-mantle peridotites as illustrated by xenoliths from basalts. J Petrol 16:454–487

Morishita T, Arai S, Green DH (2003) Evolution of low-Al orthopyroxene in the Horoman peridotite, Japan: an unusual indicator of metasomatizing fluids. J Petrol 44:1237–1246

Ohara Y, Stern RJ, Ishii T, Yurimoto H, Yamazaki T (2002) Peridotites from the Mariana Trough: first look at the mantle beneath an active back-arc basin. Contrib Mineral Petrol 143:1–18

Ozawa K (1988) Ultramafic tectonite of the Miyamori ophiolitic complex in the Kitakami Mountains, Northeast Japan: hydrous upper mantle in an island arc. Contrib Mineral Petrol 99:159–175

Ozawa K (1994) Melting and melt segregation in the mantle wedge above a subduction zone: evidence from the chromite-bearing peridotites of the Miyamori Ophiolite Complex, Northeastern Japan. J Petrol 35:647–678

Ozawa K, Shimizu N (1995) Open-system melting in the upper mantle: constraints from the Hayachine–Miyamori ophiolite, northeastern Japan. J Geophys Res 100:22,315–22,335

Parkinson IJ, Pearce JA (1998) Peridotite from the Izu-Bonin-Mariana forearc (ODP Leg 125): evidence for mantle melting and melt–mantle interaction in a supra-subduction zone setting. J Petrol 39:1577–1618

Pearson DG (1999) The age of continental roots. Lithos 48:171–194

Pollack HN, Chapman DS (1977) On the regional variation of heat flow, geotherms and lithosphere thickness. Tectonophysics 38:279–296

Ringwood AE (1966) The chemical composition and origin of the Earth. In: Hurley P (ed) Advances in earth sciences, pp 287–356

Rudnick RL, McDonough WF, Orpin A (1994) Northern Tanzanian peridotite xenoliths: a comparison with Kaapvaal peridotites and inferences on metasomatic interactions. In: Meyer HOA, Leonardos O (eds) Kimberlites, related rocks and mantle xenoliths. CPRM, Brasilia, pp 336–353

Shirey SB, Walker RJ (1995) Caries tube digestion for low-blank rhenium–osmium analysis. Anal Chem 67:2136–2141

Shirey SB, Walker RJ (1998) The Re–Os isotope system in cosmochemistry and high-temperature geochemistry. Annu Rev Earth Planet Sci 26:423–500

Smith D, Riter JCA (1997) Genesis and evolution of low-Al orthopyroxene in spinel peridotite xenoliths, Grand Canyon field, Arizona, USA. Contrib Mineral Petrol 127:391–404

Walter MJ (1998) Melting of garnet peridotite and the origin of komatiite and depleted lithosphere. J Petrol 39:29–60

Walter MJ (2003) Melt extraction and compositional variability in mantle lithosphere. Treatise Geochem 2:363–394

Witt-Eickschen G, Seck HA (1991) Solubility of Ca and Al in orthopyroxene from spinel peridotite: an improved version of an empirical geothermometer. Contrib Mineral Petrol 106:431–439